Suppression of decay widths in singly heavy baryons induced by the $U_A(1)$ anomaly

Yohei Kawakami[*] and Masayasu Harada[†]
Department of Physics, Nagoya University, Nagoya 464-8602, Japan

Makoto Oka[‡]
Advanced Science Research Center, Japan Atomic Energy Agency (JAEA), Tokai 319-1195, Japan and Nishina Center for Accelerator-Based Science, RIKEN, Wako 351-0198, Japan

Kei Suzuki[§]
Advanced Science Research Center, Japan Atomic Energy Agency (JAEA), Tokai 319-1195, Japan

(Received 22 September 2020; accepted 2 November 2020; published 1 December 2020)

We study strong and radiative decays of excited singly heavy baryons (SHBs) using an effective chiral Lagrangian based on the diquark picture proposed in Ref. [1]. The effective Lagrangian contains a $U_A(1)$ anomaly term, which induces an inverse mass ordering between strange and nonstrange SHBs with spin-parity $1/2^-$. We find that the effect of the $U_A(1)$ anomaly combined with flavor symmetry breaking modifies the Goldberger-Treiman relation for the mass difference between the ground state $\Lambda_Q(1/2^+)$ and its chiral partner $\Lambda_Q(1/2^-)$, and $\Lambda_Q(1/2^-)\Lambda_Q(1/2^+)\eta$ coupling, which results in suppression of the decay width of $\Lambda_Q(1/2^-) \to \Lambda_Q(1/2^+)\eta$. We also investigate the other various decays such as $\Lambda_Q(1/2^-) \to \Sigma_Q(1/2^+, 3/2^+)\pi\pi$, $\Lambda_Q(1/2^-) \to \Sigma_Q(1/2^+)\pi$, $\Lambda_Q(1/2^-) \to \Sigma_Q(1/2^+, 3/2^+)\gamma$, and $\Lambda_Q(1/2^-) \to \Lambda_Q(1/2^+)\pi^0$ for a wide mass range of $\Lambda_Q(1/2^-)$.

DOI: 10.1103/PhysRevD.102.114004

I. INTRODUCTION

Spontaneous chiral symmetry breaking and the $U_A(1)$ anomaly are the essential properties of quantum chromodynamics (QCD). Since colored quarks and gluons are not directly observed at the low-energy scale in QCD, verification of these properties in hadronic phenomena provides precious clues to understand the symmetry properties of QCD. Chiral partner structure of hadron spectra and the heavy η' mass spectrum are examples of such phenomena.

It is also important to interpret hadronic phenomena based on colored constitutions such as diquarks. The diquark is the simplest colored cluster that is known to play an important role in structures of baryons and exotic multiquark hadrons, and a color superconducting phase.

Singly heavy baryons (SHBs) are considered and studied as the bound states of a diquark and a heavy quark (c or b quark). Recently, diquarks made of light quarks were studied from the chiral-symmetry viewpoints, and a chiral effective theory for scalar or pseudoscalar diquarks was proposed [1]. The proposed Lagrangian contains a term representing a $U_A(1)$ anomaly effect. It is found that the term induces inverse mass ordering between strange and nonstrange SHBs with spin-parity $1/2^-$.

In this paper, we focus on investigation of decay widths of SHBs with spin-parity $1/2^-$ based on the model given in Ref. [1], and we find that the effect of a $U_A(1)$ anomaly, combined with the flavor symmetry breaking, modifies the Goldberger-Treiman (GT) relation for the mass difference between $\Lambda_Q(1/2^-)$ and $\Lambda_Q(1/2^+)$, and $\Lambda_Q(1/2^-)\Lambda_Q(1/2^+)\eta$ coupling. This modification induces suppression of the decay width of $\Lambda_Q(1/2^-) \to \Lambda_Q(1/2^+)\eta$, when the mass of $\Lambda_Q(1/2^-)$ is above the threshold of $\Lambda_Q(1/2^+)\eta$. We also study various other decay modes of $\Lambda_Q(1/2^-)$ for the mass region below the threshold such as $\Lambda_Q(1/2^-) \to \Sigma_Q(1/2^+, 3/2^+)\pi\pi$, $\Lambda_Q(1/2^-) \to \Sigma_Q(1/2^+)\pi$, $\Lambda_Q(1/2^-) \to \Sigma_Q(1/2^+, 3/2^+)\gamma$, and $\Lambda_Q(1/2^-) \to \Lambda_Q(1/2^+)\pi^0$. Finally, we mention decays of $\Xi_Q(1/2^-)$ based on the model.

[*]kawakami@hken.phys.nagoya-u.ac.jp
[†]harada@hken.phys.nagoya-u.ac.jp
[‡]oka@post.j-parc.jp
[§]k.suzuki.2010@th.phys.titech.ac.jp

This paper is organized as follows: We show the masses and GT relations obtained in the model in Sec. II. Section III is devoted to the study of the effect of the $U_A(1)$ anomaly on $\Lambda_Q(1/2^-) \to \Lambda_Q(1/2^+)\eta$ decay. We study the other decays of $\Lambda_Q(1/2^-)$ in Sec. IV. Finally, we give a summary and discussions in Sec. V.

II. MASSES AND GOLDBERGER-TREIMAN RELATIONS

In Ref. [1], a chiral effective Lagrangian of scalar and pseudoscalar diquarks based on chiral $SU(3)_R \times SU(3)_L$ symmetry is proposed. Each diquark forms a SHB as a bound state to a heavy quark $Q(c/b)$ which belongs to the flavor $\bar{3}$ representation ($\Lambda_{c/b}$ or $\Xi_{c/b}$). In this paper, we express those SHBs by linear representations: $S_{R,i}$ ($i = 1, 2, 3$) belongs to the $(\bar{3}, 1)$ representation under $SU(3)_R \times SU(3)_L$ symmetry, and $S_{L,i}$ to $(1, \bar{3})$. The effective Lagrangian of the SHBs in the chiral limit is given as

$$\begin{aligned}\mathcal{L} = {} & \bar{S}_{R,i}(iv^\mu\partial_\mu)S_{R,i} + \bar{S}_{L,i}(iv^\mu\partial_\mu)S_{L,i} \\ & - M_{B0}(\bar{S}_{R,i}S_{R,i} + \bar{S}_{L,i}S_{L,i}) \\ & - \frac{M_{B1}}{f}(\bar{S}_{R,i}\Sigma^T_{ij}S_{L,j} + \bar{S}_{L,i}\Sigma^{T\dagger}_{ij}S_{R,j}) \\ & - \frac{M_{B2}}{2f^2}\epsilon_{ijk}\epsilon_{lmn}(\bar{S}_{L,k}\Sigma^T_{li}\Sigma^T_{mj}S_{R,n} + \bar{S}_{R,k}\Sigma^{T\dagger}_{li}\Sigma^{T\dagger}_{mj}S_{L,n}),\end{aligned} \tag{1}$$

where v^μ is the velocity of SHBs; M_{B0}, M_{B1}, and M_{B2} are model parameters; $f = 92.4$ MeV is the pion decay constant; the indices i, j, k, l, m, $n = 1, 2, 3$ are for either $SU(3)_R$ or $SU(3)_L$; and summations over repeated indices are understood. Here, Σ_{ij} denotes the effective field for light scalar and pseudoscalar mesons belonging to the chiral $(\bar{3}, 3)$ representation. These fields transform as

$$\Sigma_{ij} \to U_{L,ik}\Sigma_{kl}U^\dagger_{R,lj}, \tag{2}$$

$$S_{R,i} \to U^\dagger_{R,ji}S_{R,j}, \qquad S_{L,i} \to U^\dagger_{L,ji}S_{L,j}. \tag{3}$$

The Lagrangian is invariant under these chiral transformations. In addition, the kinetic, M_{B0}, and M_{B2} terms are also invariant under the following $U_A(1)$ transformations:

$$\Sigma_{ij} \to e^{-2i\theta}\Sigma_{ij}, \tag{4}$$

$$S_{R,i} \to e^{2i\theta}S_{R,i}, \qquad S_{L,i} \to e^{-2i\theta}S_{L,i}. \tag{5}$$

In contrast, the M_{B1} term is not invariant under these transformations, reflecting the $U_A(1)$ anomaly.

The chiral symmetry is spontaneously broken by the vacuum expectation values of the Σ_{ij} field as $\langle\Sigma_{ij}\rangle = f\delta_{ij}$. Then, the M_{B1} and M_{B2} terms give contributions to the mass splitting between parity eigenstates of SHBs defined as

$$S_i = \frac{1}{\sqrt{2}}(S_{R,i} - S_{L,i}) = \begin{cases} \Xi_Q(1/2^+) & (i = 1, 2) \\ \Lambda_Q(1/2^+) & (i = 3), \end{cases} \tag{6}$$

$$P_i = \frac{1}{\sqrt{2}}(S_{R,i} + S_{L,i}) = \begin{cases} \Xi_Q(1/2^-) & (i = 1, 2) \\ \Lambda_Q(1/2^-) & (i = 3). \end{cases} \tag{7}$$

In this paper, we follow the prescription adopted in Ref. [1], in which the explicit breaking of flavor symmetry is introduced by the replacement

$$\Sigma \to \tilde{\Sigma} \equiv \Sigma + \mathrm{diag}\{0, 0, (A-1)f\}, \tag{8}$$

with $A \sim 5/3$ being the parameter of flavor breaking. The vacuum expectation value of $\tilde{\Sigma}$ is given by

$$\langle\tilde{\Sigma}\rangle = f\mathrm{diag}(1, 1, A). \tag{9}$$

Then, the masses of the SHBs are expressed as

$$M^\pm_{1,2} = M_{B0} \mp (M_{B1} + AM_{B2}), \tag{10}$$

$$M^\pm_3 = M_{B0} \mp (AM_{B1} + M_{B2}), \tag{11}$$

where $M^\pm_{1,2}$ denote the masses of $\Xi_Q(1/2^+)$ and $\Xi_Q(1/2^-)$, and $M^\pm_3$ the masses of $\Lambda_Q(1/2^+)$ and $\Lambda_Q(1/2^-)$. From Eqs. (10) and (11), we obtain mass differences between chiral partners as

$$\Delta M_{1,2} = 2(M_{B1} + AM_{B2}), \tag{12}$$

$$\Delta M_3 = 2(AM_{B1} + M_{B2}). \tag{13}$$

We require $M^+_{1,2} > M^+_3$ consistently with the experimental values of the masses of the ground-state SHBs. The inverse mass ordering between strange and nonstrange SHBs proposed in Ref. [1] indicates $M^-_{1,2} < M^-_3$; then we obtain a relation $\Delta M_{1,2} < \Delta M_3$. For this relation, the effect of the anomaly plays a crucial role. When we ignore M_{B1} in Eqs. (10)–(13), the realistic mass ordering of SHBs ($M^+_{1,2} < M^-_{1,2}$ and $M^+_3 < M^-_3$) results in $M_{B2} > 0$. Then, $M_{B2} > 0$, together with $A > 1$, leads to $\Delta M_{1,2} > \Delta M_3$.

Next, we study the couplings among chiral partners and a pseudo-Nambu-Goldstone (pNG) boson. For this purpose, we introduce light scalar mesons σ_{ij} and pseudoscalar mesons π_{ij} as

$$\tilde{\Sigma}_{ij} = \langle\tilde{\Sigma}_{ij}\rangle + \sigma_{ij} + i\pi_{ij}, \tag{14}$$

with

$$\pi_{ij} = \sqrt{2}\begin{pmatrix} \frac{\pi^0}{\sqrt{2}} + \frac{\eta_8}{\sqrt{6}} + \frac{\eta_1}{\sqrt{3}} & \pi^+ & K^+ \\ \pi^- & -\frac{\pi^0}{\sqrt{2}} + \frac{\eta_8}{\sqrt{6}} + \frac{\eta_1}{\sqrt{3}} & K^0 \\ K^- & \bar{K}^0 & -\frac{2\eta_8}{\sqrt{6}} + \frac{\eta_1}{\sqrt{3}} \end{pmatrix}. \tag{15}$$

The M_{B1} and M_{B2} terms of the Lagrangian (1) provide interactions of the SHBs with light mesons. In the chiral limit ($A = 1$), we obtain the relation between the coupling constant for the interaction of SHBs with a pNG boson $g_{\pi SP}$ and the mass difference of SHBs ΔM as

$$g_{\pi SP} = \frac{M_{B1} + M_{B2}}{f} = \frac{\Delta M}{2f}. \tag{16}$$

This is often called the extended GT relation. We focus on studying the coupling of $\Lambda_Q(1/2^-)\Lambda_Q(1/2^+)\eta$ in this section, and we use g for the coupling constant below. When the flavor symmetry breaking is included using $A > 1$, the coupling constant is obtained as

$$g = \frac{M_{B1} + M_{B2}}{f} = \frac{\Delta M_{1,2} + \Delta M_3}{2f(A+1)}. \tag{17}$$

From inverse mass ordering, we obtain $\Delta M_{1,2} < \Delta M_3$ as we showed above. Then, we see that

$$g = \frac{\Delta M_3}{2f}\frac{\frac{\Delta M_{1,2}}{\Delta M_3} + 1}{A+1} < \frac{\Delta M_3}{2f}, \tag{18}$$

which indicates that the value of the coupling constant is smaller than the one expected from the GT relation. In order to see that this is caused by the effect of the anomaly, we drop M_{B1} in Eqs. (13) and (17). Then, we obtain the coupling constant as

$$\bar{g} = \frac{M_{B2}}{f} = \frac{\Delta M_3}{2f}, \tag{19}$$

which is the one expected from the GT relation in Eq. (16). Therefore, we conclude that the $U_A(1)$ anomaly suppresses the value of the coupling constant. This suppression is expected to be seen in the decay width of $\Lambda_Q(1/2^-) \to \Lambda_Q(1/2^+)\eta$.

III. EFFECT OF ANOMALY ON $\Lambda_Q(1/2^-) \to \Lambda_Q(1/2^+)\eta$ DECAY

In this section, we numerically study how the effect of the anomaly suppresses the decay of $\Lambda_Q(1/2^-) \to \Lambda_Q(1/2^+)\eta$. Interaction among $\Lambda_Q(1/2^-)$, $\Lambda_Q(1/2^+)$, and η_8 or η_1 is obtained from the Lagrangian (1) as

$$i\frac{2}{\sqrt{3}}\left\{\frac{M_{B1}}{f}\left(\eta_8 - \frac{1}{\sqrt{2}}\eta_1\right) + \frac{M_{B2}}{f}(\eta_8 + \sqrt{2}\eta_1)\right\} \cdot \bar{\Lambda}_Q(1/2^+)\Lambda_Q(1/2^-), \tag{20}$$

where η_8 is a member of the octet of $SU(3)$ flavor symmetry, and η_1 belongs to the flavor singlet. The realistic η is known as a mixing state of η_8 and η_1. As shown in the previous section, although η_8 is a pNG boson associated with the chiral $SU(3)_R \times SU(3)_L$ symmetry breaking, its coupling constant to $\Lambda_c(1/2^-)$ and $\Lambda_c(1/2^+)$ given in Eq. (17) is smaller than the naive expectation of the GT relation in Eq. (16). On the other hand, the coupling constant of η_1 is read from Lagrangian (1) as

$$g_{\eta_1} = \frac{M_{B1} - 2M_{B2}}{f}. \tag{21}$$

This is also different from the GT relation since η_1 is no longer a pNG boson when the effect of the $U_A(1)$ anomaly is included. In the following, we first see that the coupling constant in Eq. (17) is suppressed compared with the one in Eq. (19) due to the effect of the anomaly, as shown in Eq. (18) by regarding η_8 as η and neglecting small mixing between η and η'. The effect of the η-η' mixing is introduced for comparison with the realistic decay width afterward. The values of M_{B1} and M_{B2} in Eq. (17) are determined from the masses of $\Lambda_c(1/2^-)$, $\Lambda_c(1/2^+)$, and $\Xi_c(1/2^+)$. We use the experimental values of the masses of $\Lambda_c(1/2^+)$ and $\Xi_c(1/2^+)$ as $M(\Lambda_c(1/2^+)) = 2286.46$ MeV and $M(\Xi_c(1/2^+)) = 2469.42$ MeV.[1] Since the mass of $\Lambda_c(1/2^-)$ is not determined in experiment, we calculate the decay width for a wide range of the mass of $\Lambda_c(1/2^-)$. We note that, although $\Lambda_c(2595)$ carries $J^P = 1/2^-$, it is not $\Lambda_c(1/2^-)$ here since $\Lambda_c(2595)$ results in a heavy-quark spin doublet with $\Lambda_c(2625)$ having $3/2^-$.

We show the decay width of $\Lambda_c(1/2^-) \to \Lambda_c(1/2^+)\eta$ in Fig. 1. The thin solid green and thin dotted orange curves are plotted without η-η' mixing. The thin solid green curve is drawn by using the coupling constant in Eq. (17) which includes the effect of the anomaly, while the thin dotted orange curve is drawn by using the one in Eq. (19) without the anomaly. One can easily see that the thin solid green curve is quite suppressed compared with the thin dotted orange curve.

Next, let us include the effect of η-η' mixing. Introducing the η-η' mixing matrix as [3]

$$\begin{pmatrix} \eta \\ \eta' \end{pmatrix} = \begin{pmatrix} \cos\theta_P & -\sin\theta_P \\ \sin\theta_P & \cos\theta_P \end{pmatrix}\begin{pmatrix} \eta_8 \\ \eta_1 \end{pmatrix}, \tag{22}$$

[1]When we calculate the coupling constant in Eq. (19), we do not use the mass of $\Xi_c(1/2^+)$ as an input.

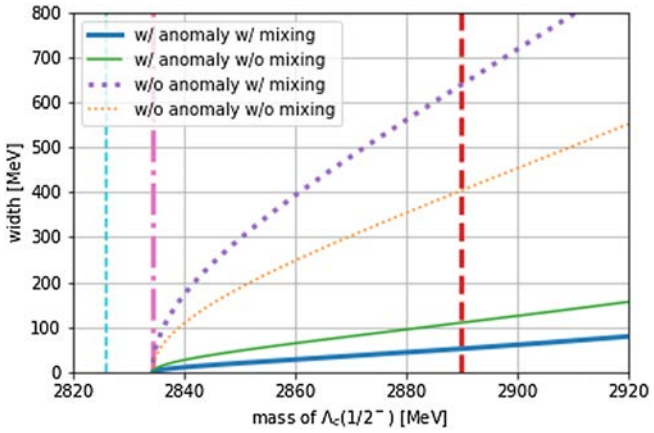

FIG. 1. Dependence of $\Lambda_c(1/2^-) \to \Lambda_c(1/2^+)\eta$ width on the mass of $\Lambda_c(1/2^-)$. Predictions without the η-η' mixing are shown by the thin solid green (with anomaly) and thin dotted orange (without anomaly) curves, and those with the η-η' mixing are shown by the thick solid blue and thick dotted purple curves. Two predictions of the mass of $\Lambda_c(1/2^-)$ are shown by the vertical thick dashed red [2] and thin dashed cyan [1] lines. The thick-dash-dotted magenta line shows the threshold of $\Lambda_c(1/2^+)\eta$ (~2834 MeV).

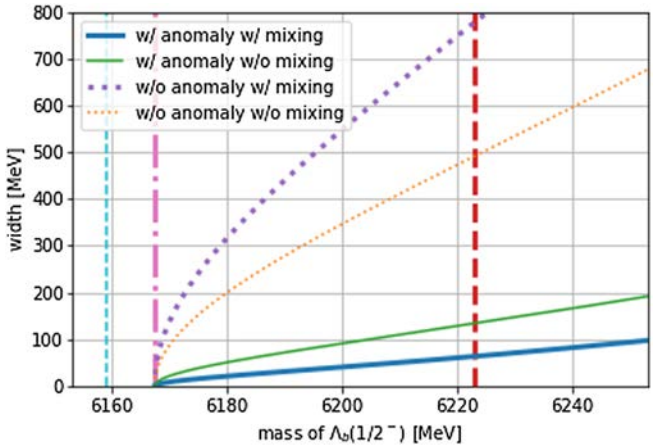

FIG. 2. Dependence of $\Lambda_b(1/2^-) \to \Lambda_b(1/2^+)\eta$ width on the mass of $\Lambda_b(1/2^-)$. Curves in this figure respectively correspond to those in Fig. 1. See the main text for the vertical lines.

the $\Lambda_Q(1/2^-)\Lambda_Q(1/2^+)\eta$ interaction is obtained from Eq. (20) as

$$i\frac{2}{\sqrt{3}}g_{\rm phys}\bar{\Lambda}_Q(1/2^+)\Lambda_Q(1/2^-)\eta, \tag{23}$$

where

$$g_{\rm phys} = \frac{\xi_1 M_{B1} + \xi_2 M_{B2}}{f}, \tag{24}$$

with $\xi_1 = \cos\theta_P + \sin\theta_P/\sqrt{2}$ and $\xi_2 = \cos\theta_P - \sqrt{2}\sin\theta_P$. Here, we use $\theta_P = -11.3°$ listed in Ref. [3]. In Fig. 1, the thick solid blue curve shows the width of $\Lambda_c(1/2^-) \to \Lambda_c(1/2^+)\eta$ decay calculated by using the coupling constant in Eq. (24). Comparing with the thin solid green curve, we see that the effect of η-η' mixing suppresses the decay width by about 50%. When the effect of the anomaly is dropped by taking $M_{B1} = 0$, the coupling constant in Eq. (24) is reduced to

$$\bar{g}_{\rm phys} = \frac{\xi_2 M_{B2}}{f} = \xi_2 \bar{g}. \tag{25}$$

Since $\xi_2 \sim 1.26$, the above relation implies that the width is enhanced by about 60%, as shown by the thick dotted purple curve compared with the thin dotted orange curve in Fig. 1.

At the end of this section, let us apply our analysis to the bottom sector. The parameters M_{B1} and M_{B2} of the Lagrangian (1) are uniquely determined when the mass of $\Lambda_c(1/2^-)$ on the horizontal axis in Fig. 1 is fixed. Here, we apply the Lagrangian (1) to the bottom sector and use the values of M_{B1} and M_{B2} determined above to evaluate the mass difference between $\Lambda_b(1/2^+)$ and $\Lambda_b(1/2^-)$, and the decay width of $\Lambda_b(1/2^-) \to \Lambda_b(1/2^+)\eta$. The mass difference between $\Lambda_b(1/2^+)$ and $\Lambda_b(1/2^-)$ is equal to that between $\Lambda_c(1/2^+)$ and $\Lambda_c(1/2^-)$. We show the resultant decay width in Fig. 2. In this figure, the vertical thick dashed red line shows $M(\Lambda_b, 1/2^-) = 6223$ MeV determined by using $M(\Lambda_c, 1/2^-) = 2890$ MeV [2] as an input, and the vertical thin dashed cyan line is for $M(\Lambda_b, 1/2^-) = 6159$ MeV by using $M(\Lambda_c, 1/2^-) = 2826$ MeV [1]. The vertical thick dash-dotted magenta line shows the threshold of $\Lambda_b(1/2^+)\eta$. We can see that the effect of the anomaly suppresses the decay widths as in the charm sector. Similarly, the effect of η-η' mixing enhances the decay width in the case without the anomaly and suppresses that with the anomaly. We also observe that all the decay widths of $\Lambda_b(1/2^-)$ in Fig. 2 are enhanced compared with those of $\Lambda_c(1/2^-)$ in Fig. 1. This is caused by the kinematical factor, although the relevant coupling constants are equal to each other.

IV. OTHER DECAYS OF $\Lambda_Q(1/2^-)$

The mass of $\Lambda_Q(1/2^-)$ ($Q = c$, b) has not yet been experimentally determined. When it is larger than the threshold of $\Lambda_Q(1/2^-)\eta$, $\Lambda_Q(1/2^-) \to \Lambda_Q(1/2^+)\eta$ decay is expected to be dominant. On the other hand, if $\Lambda_Q(1/2^-)$ is located below the threshold as predicted in Refs. [1,4], other decay modes become relevant. Then, we investigate the decays of $\Lambda_Q(1/2^-) \to \Sigma_Q^{(*)}\pi\pi$, $\Lambda_Q(1/2^-) \to \Sigma_Q^{(*)}\gamma$, $\Lambda_Q(1/2^-) \to \Sigma_Q\pi$, and $\Lambda_Q(1/2^-) \to \Lambda_Q(1/2^+)\pi^0$ [Σ_Q and Σ_Q^* denote $\Sigma_Q(1/2^+)$ and $\Sigma_Q(3/2^+)$, respectively].

We expect that $\Lambda_Q(1/2^-) \to \Sigma_Q^{(*)}\pi\pi$ decay becomes large when the mass of $\Lambda_Q(1/2^-)$ is far above the threshold

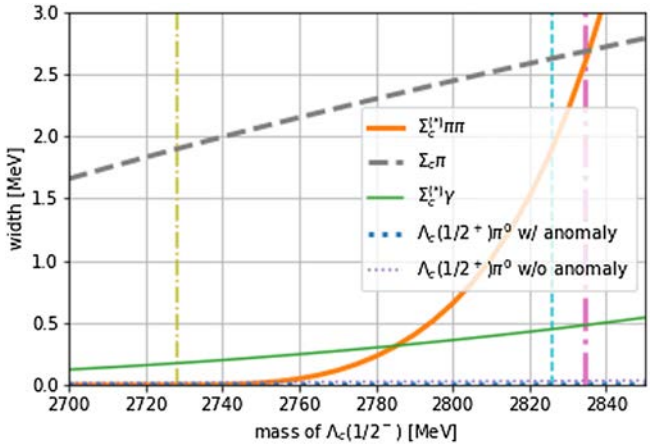

FIG. 3. Dependence of various decay widths of $\Lambda_c(1/2^-)$ on the mass of $\Lambda_c(1/2^-)$. The thick solid orange, thick dashed gray, and thin solid green curves, respectively, show $\Gamma_{\Sigma_c^{(*)}\pi\pi}/k^2$, $\Gamma_{\Sigma_c\pi}/\kappa^2$, and $\Gamma_{\Sigma_c^{(*)}\gamma}/r^2$. The thick dotted blue and thin dotted purple curves show the width of $\Lambda_c(1/2^-) \to \Lambda_c(1/2^+)\pi^0$ with the coupling constant in Eq. (26) (with anomaly) and in Eq. (27) (without anomaly). The vertical thick dash-dotted magenta and thin dashed cyan lines correspond to those in Fig. 1. The vertical thin dash-dotted olive line shows the threshold of $\Sigma_c\pi\pi$.

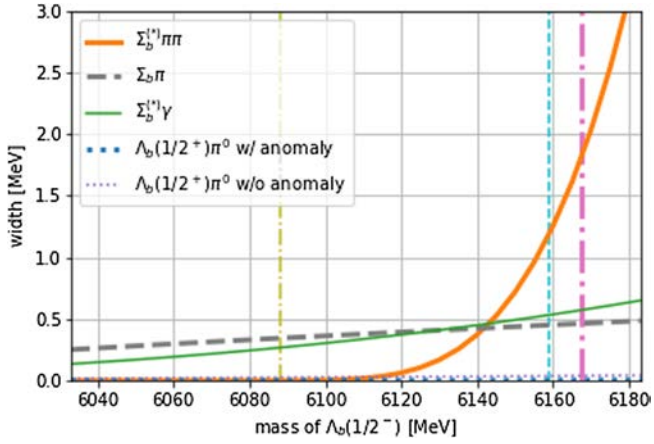

FIG. 4. Dependence of various decay widths of $\Lambda_b(1/2^-)$ on the mass of $\Lambda_b(1/2^-)$. The curves correspond to those in Fig. 3. The vertical thick dash-dotted magenta and thin dashed cyan lines correspond to those in Fig. 2. The vertical thin dash-dotted olive line shows the threshold of $\Sigma_b\pi\pi$.

of $\Lambda_Q(1/2^-) \to \Sigma_Q\pi\pi$, and that the radiative decay is suppressed. Although $\Lambda_Q(1/2^-) \to \Sigma_Q\pi$ decay violates the heavy-quark symmetry, it can be dominant near the threshold of $\Lambda_Q(1/2^-) \to \Sigma_Q\pi\pi$, especially in the charm sector. Note that $\Lambda_Q(1/2^-) \to \Lambda_Q(1/2^+)\pi^0$ will be strongly suppressed since it breaks isospin symmetry.

Typical forms of interaction Lagrangians are given in Appendix A. The coupling constant of $\Lambda_Q(1/2^-) \to \Sigma_Q^{(*)}\pi\pi$ is estimated as $k = 1$ by the ρ meson dominance and the coupling universality [5–7], but so far we cannot precisely determine its value using the known experimental data of SHBs. Furthermore, the coupling constants of $\Lambda_Q(1/2^-) \to \Sigma_Q\pi$ and $\Lambda_Q(1/2^-) \to \Sigma_Q^{(*)}\gamma$ are unknown. We therefore leave k, κ, and r as free parameters.

We show the dependence of estimated widths on the mass of $\Lambda_c(1/2^-)$ in Fig. 3. We also show the estimated widths of $\Lambda_b(1/2^-)$ in Fig. 4. We note that these figures show the decay widths of $\Lambda_Q(1/2^-) \to \Sigma_Q^{(*)}\pi\pi$, $\Lambda_Q(1/2^-) \to \Sigma_Q\pi$, and $\Lambda_Q(1/2^-) \to \Sigma_Q^{(*)}\gamma$ divided by the unknown constants k^2, κ^2, and r^2, respectively. On the other hand, the $\Lambda_Q(1/2^-) \to \Lambda_Q(1/2^+)\pi^0$ mode is completely determined by the chiral property in the present analysis, so the decay width itself is plotted.

We see that decay widths of $\Lambda_Q(1/2^-) \to \Sigma_Q^{(*)}\pi\pi$, $\Lambda_Q(1/2^-) \to \Sigma_Q^{(*)}\gamma$, and $\Lambda_Q(1/2^-) \to \Lambda_Q(1/2^+)\pi^0$ in the charm sector are almost the same as those in the bottom sector. On the other hand, the decay width of $\Lambda_b(1/2^-) \to \Sigma_b\pi$ is very suppressed compared with that of $\Lambda_c(1/2^-) \to \Sigma_c\pi$ since the heavy-quark symmetry is well satisfied in the bottom sector.

Figure 3 shows that, below the threshold of $\Lambda_c(1/2^+)\eta$ indicated by the vertical thick dash-dotted magenta line, the dominant decay mode is $\Lambda_c(1/2^-) \to \Sigma_c\pi$, shown by the thick-dashed gray curve, which violates the heavy-quark symmetry. Figure 4 shows that, below the threshold, the dominant decay mode is $\Lambda_b(1/2^-) \to \Sigma_b^{(*)}\pi\pi$, indicated by the thick solid orange curve. When the mass of $\Lambda_b(1/2^-)$ is a little above the threshold of $\Lambda_b(1/2^-) \to \Sigma_b\pi\pi$ indicated by the vertical thin dash-dotted olive line, $\Lambda_b(1/2^-) \to \Sigma_b^{(*)}\pi\pi$ decay is suppressed, and $\Lambda_b(1/2^-) \to \Sigma_b\pi$ and $\Lambda_b(1/2^-) \to \Sigma_b^{(*)}\gamma$ decays are dominant. Since $\Lambda_b(1/2^-) \to \Sigma_b\pi$ decay is strongly suppressed by the heavy-quark symmetry in the bottom sector, the width is comparable to that of the radiative decay.

Note that $\Lambda_Q(1/2^-) \to \Lambda_Q(1/2^+)\pi^0$ decay originates from $\pi^0 - \eta$ mixing generated by the isospin violation. The coupling constant of $\Lambda_Q(1/2^-) \to \Lambda_Q(1/2^+)\pi^0$ is written as

$$g_{\pi^0\eta} = \Delta_{\pi^0\eta} g_{\rm phys}, \tag{26}$$

where $\Delta_{\pi^0\eta}$ is a parameter of $\pi^0 - \eta$ mixing estimated as $\Delta_{\pi^0\eta} \sim -5.32 \times 10^{-3}$ in Ref. [8] with a scheme given in Ref. [9]. Similarly, we obtain

$$\bar{g}_{\pi^0\eta} = \Delta_{\pi^0\eta} \bar{g}_{\rm phys}. \tag{27}$$

Predicted widths from Eq. (26) are shown by thick dotted blue curves in Figs. 3 and 4, and those from Eq. (27) are

TABLE I. Decay widths of $\Lambda_c(1/2^-)$ without and with the effect of the anomaly. Units of masses and widths are in MeV. The last two rows show the numerical values of the total widths without and with an anomaly, respectively, under the arbitrary assumptions $k = 1$, $\kappa = 1$, and $r = 1$.

Mass of $\Lambda_c(1/2^-)$ [MeV]	2702 [4]	2759 [4]	2826 [1]	2890 [2]
$\Lambda_c(1/2^-) \to \Lambda_c(1/2^+)\eta$ without anomaly	⋯	⋯	⋯	639
$\Lambda_c(1/2^-) \to \Lambda_c(1/2^+)\eta$ with anomaly	⋯	⋯	⋯	52.3
$\Lambda_c(1/2^-) \to \Sigma_c^{(*)}\pi\pi$	⋯	$0.0400k^2$	$1.84k^2$	$13.0k^2$
$\Lambda_c(1/2^-) \to \Sigma_c\pi$	$1.67\kappa^2$	$2.14\kappa^2$	$2.62\kappa^2$	$3.04\kappa^2$
$\Lambda_c(1/2^-) \to \Sigma_c^{(*)}\gamma$	$0.126r^2$	$0.243r^2$	$0.448r^2$	$0.718r^2$
$\Lambda_c(1/2^-) \to \Lambda_c(1/2^+)\pi^0$ without anomaly	0.0147	0.0213	0.0309	0.0422
$\Lambda_c(1/2^-) \to \Lambda_c(1/2^+)\pi^0$ with anomaly	2.60×10^{-4}	7.87×10^{-4}	1.87×10^{-3}	3.46×10^{-3}
Total without anomaly	1.81	2.44	4.93	656
Total with anomaly	1.80	2.42	4.90	69.0

TABLE II. Decay widths of $\Lambda_b(1/2^-)$ without and with the effect of the anomaly. Units of masses and widths are in MeV. Note that "6159 MeV" is not listed in Ref. [1], but it is estimated in the same way as the prediction "2826 MeV" in Table I. The last two rows show the numerical values of the total widths without and with an anomaly, respectively, under the arbitrary assumptions $k = 1$, $\kappa = 1$, and $r = 1$.

Mass of $\Lambda_b(1/2^-)$ [MeV]	5999 [4]	6079 [4]	6159 [1]	6174 [4]	6207 [4]
$\Lambda_b(1/2^-) \to \Lambda_b(1/2^+)\eta$ without anomaly	⋯	⋯	⋯	223	619
$\Lambda_b(1/2^-) \to \Lambda_b(1/2^+)\eta$ with anomaly	⋯	⋯	⋯	16.5	52.9
$\Lambda_b(1/2^-) \to \Sigma_b^{(*)}\pi\pi$	⋯	⋯	$1.16k^2$	$2.38k^2$	$7.95k^2$
$\Lambda_b(1/2^-) \to \Sigma_b\pi$	$0.183\kappa^2$	$0.329\kappa^2$	$0.450\kappa^2$	$0.472\kappa^2$	$0.518\kappa^2$
$\Lambda_b(1/2^-) \to \Sigma_b^{(*)}\gamma$	$0.0795r^2$	$0.241r^2$	$0.531r^2$	$0.603r^2$	$0.781r^2$
$\Lambda_b(1/2^-) \to \Lambda_b(1/2^+)\pi^0$ without anomaly	0.0129	0.0229	0.0369	0.0400	0.0473
$\Lambda_b(1/2^-) \to \Lambda_b(1/2^+)\pi^0$ with anomaly	9.50×10^{-5}	7.41×10^{-4}	2.23×10^{-3}	2.62×10^{-3}	3.63×10^{-3}
Total without anomaly	0.275	0.593	2.18	226	628
Total with anomaly	0.263	0.571	2.14	20.0	62.2

shown by thin dotted purple curves for comparison. We see that these decay widths are very small.

V. SUMMARY AND DISCUSSIONS

In this paper, we study strong and radiative decays of excited SHBs using a chiral effective Lagrangian based on the diquark picture proposed in Ref. [1]. We show predictions of widths for typical choices of the mass of $\Lambda_Q(1/2^-)$ in Tables I and II. Our prediction on the width of $\Lambda_Q(1/2^-) \to \Lambda_Q(1/2^+)\eta$ is strongly suppressed by the effect of the anomaly compared with the prediction without an anomaly. In general, the large width of the chiral partner state is an obstacle to its observation. The suppression of the width may enable us to observe the state easily. Tables I and II also show predictions on the other decay modes, which are useful for experimental observation of chiral partners when the mass of $\Lambda_Q(1/2^-)$ is located below the threshold of $\Lambda_Q(1/2^+)\eta$. For illustrative purposes, in the last two rows of Tables I and II, we show the numerical values of the total widths without and with an anomaly, respectively, under the arbitrary assumptions $k = 1$, $\kappa = 1$, and $r = 1$.

In the chiral partner structure using (3, 3) representations for the diquark with $J^P = 1^\pm$, the chiral partners to $\Sigma_Q(J^P = 1/2^+)$ and $\Sigma_Q^*(3/2^+)$ are $\Lambda_{Q1}(1/2^-)$ and $\Lambda_{Q1}^*(3/2^-)$, respectively, as in Eq. (A1) in Appendix A. In such a case, $\Lambda_Q(1/2^-) \to \Sigma_Q^{(*)}\gamma$ decays share a common coupling constant with $\Lambda_{Q1}^{(*)} \to \Lambda_Q(1/2^+)\gamma$ decays. Once the chiral partner $\Lambda_{Q1}^{(*)}$ is identified with some physical particles such as in Refs. [10,11], we can check the chiral partner by looking at the radiative decays of those particles.

In Tables I and II, we see that the decay width of $\Lambda_Q(1/2^-) \to \Lambda_Q(1/2^+)\pi^0$ is small. Even though it might be difficult to observe this decay experimentally, it may give some information about the $U_A(1)$ anomaly since its coupling constant is completely determined by the relation

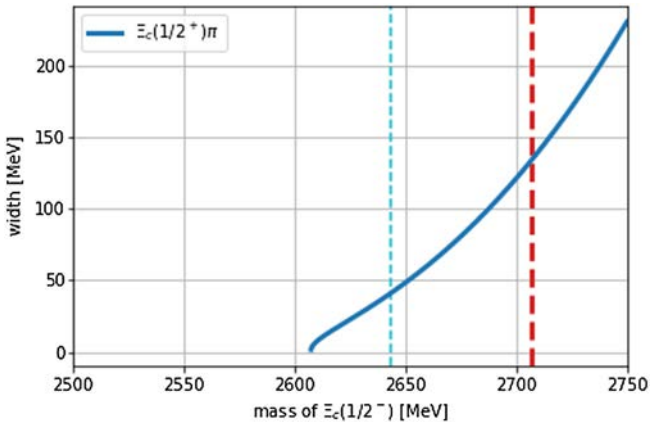

FIG. 5. Dependence of the $\Xi_c(1/2^-) \to \Xi_c(1/2^+)\pi$ width on the mass of $\Xi_c(1/2^-)$. The vertical thick dashed red line shows a prediction of the mass of $\Xi_c(1/2^-)$ (2707 MeV) calculated from Eq. (28) using $M(\Lambda_c(1/2^-)) = 2890$ MeV predicted in Ref. [2], and the vertical thin dashed cyan line shows a prediction (2643 MeV) using $M(\Lambda_c(1/2^-)) = 2826$ MeV from Ref. [1].

reflecting chiral symmetry, as shown in Eq. (26) or (27), and the width with the anomaly is strongly suppressed. Then, we may check the effect of the anomaly through this decay when the mass of $\Lambda_Q(1/2^-)$ is located below the threshold of $\Lambda_Q(1/2^+)\eta$.

The suppression of the decay width by the effect of the anomaly can also be seen at the diquark level, which we show in Appendix B.

We consider the mass and the decay width of $\Xi_c(1/2^-)$.[2] From Eqs. (10) and (11), we obtain

$$M(\Xi_c(1/2^-)) = M(\Lambda_c(1/2^+)) + M(\Lambda_c(1/2^-)) - M(\Xi_c(1/2^+)), \tag{28}$$

which determines the mass of $\Xi_c(1/2^-)$, once the mass of $\Lambda_c(1/2^-)$ is fixed. The dominant decay of $\Xi_c(1/2^-)$ is $\Xi_c(1/2^-) \to \Xi_c(1/2^+)\pi$, and the coupling constant is obtained from the Lagrangian (1) as

$$g_{\Xi_c} = \frac{M_{B1} + AM_{B2}}{f} = \frac{\Delta M_{1,2}}{2f}. \tag{29}$$

This is the same as the extended GT relation in Eq. (16). We plot the resultant relation between the mass of $\Xi_c(1/2^-)$ and the decay width of $\Xi_c(1/2^-) \to \Xi_c(1/2^+)\pi$ in Fig. 5. The vertical thick dashed red and thin dashed cyan lines correspond to those in Fig. 1: The thick dashed red line shows $M(\Xi_c(1/2^-)) = 2707$ MeV obtained from $M(\Lambda(1/2^-)) = 2890$ MeV through Eq. (28); the thin dashed cyan line shows $M(\Xi_c(1/2^-)) = 2643$ MeV from $M(\Lambda(1/2^-)) = 2826$ MeV. The mass difference between $\Xi(1/2^+)$ and $\Xi(1/2^-)$ reflecting the inverse mass hierarchy makes the phase space and the coupling constant small.

In the present analysis, we included only the leading order of the flavor symmetry breaking parameter; i.e., contributions are linear in A. Furthermore, when the effect of heavy-quark symmetry violation is included, $\Lambda_Q(1/2^-)$ can contain other diquark components which have different chiral properties [12]. We leave the study of higher orders of flavor symmetry breaking and mixing between different diquark components for future work.

ACKNOWLEDGMENTS

This work is supported in part by JSPS KAKENHI Grants No. 20K03927 (M. H.), No. 17K14277 (K. S.), No. 20K14476 (K. S.), and No. 19H05159 (M. O.).

APPENDIX A: CHIRAL (3, 3) REPRESENTATION FOR SHB AND LAGRANGIAN

To discuss various transitions of $\Lambda_Q(1/2^-)$ below the threshold of $\Lambda_Q(1/2^+)\eta$, we introduce the heavy-quark spin doublet $\Sigma_Q^{(*)}$ as a member of the chiral (3, 3) field S_{ij}^{μ} (see, e.g., Refs. [10,11] for a detailed discussion), which transforms as

$$S_{ij}^{\mu} = \hat{B}_{ij}^{6\mu} + \hat{B}_{ij}^{\bar{3}\mu} \to U_{R,ik} U_{L,jl} S_{kl}^{\mu}, \tag{A1}$$

where $\hat{B}_{ij}^{6\mu}$ is a doublet of $(1/2^+, 3/2^+)$ and $\hat{B}_{ij}^{\bar{3}\mu}$ is a doublet of $(1/2^-, 3/2^-)$. They are defined as matrix representations:

$$\hat{B}^{6\mu} = \begin{pmatrix} \Sigma_Q^{I_3=1\mu} & \frac{1}{\sqrt{2}}\Sigma_Q^{I_3=0\mu} & \frac{1}{\sqrt{2}}\Xi_Q^{\prime I_3=\frac{1}{2}\mu} \\ \frac{1}{\sqrt{2}}\Sigma_Q^{I_3=0\mu} & \Sigma_Q^{I_3=-1\mu} & \frac{1}{\sqrt{2}}\Xi_Q^{\prime I_3=-\frac{1}{2}\mu} \\ \frac{1}{\sqrt{2}}\Xi_Q^{\prime I_3=\frac{1}{2}\mu} & \frac{1}{\sqrt{2}}\Xi_Q^{\prime I_3=-\frac{1}{2}\mu} & \Omega_Q^{\mu} \end{pmatrix}, \tag{A2}$$

$$\hat{B}^{\bar{3}\mu} = \frac{1}{\sqrt{2}} \begin{pmatrix} 0 & \Lambda_{Q1}^{\mu} & \Xi_{Q1}^{I_3=\frac{1}{2}\mu} \\ -\Lambda_{Q1}^{\mu} & 0 & \Xi_{Q1}^{I_3=-\frac{1}{2}\mu} \\ -\Xi_{Q1}^{I_3=\frac{1}{2}\mu} & -\Xi_{Q1}^{I_3=-\frac{1}{2}\mu} & 0 \end{pmatrix}. \tag{A3}$$

The Lagrangian of the interactions relevant for the present analysis is written as

[2]It should be noted here that the relevant chiral partner state, $\Xi_c(1/2^-)$, is a singlet state for the heavy quark spin symmetry. Therefore, the known $\Xi_c(2790)(1/2^-)$ may not be a candidate as it seems to form a heavy-quark spin doublet with $\Xi_c(2815)(3/2^-)$.

$$\begin{aligned}\mathcal{L}_{\rm int} =& +\frac{k}{8f^3}\epsilon_{ijk}[\Sigma^T_{il}\bar{S}^\mu_{lm}(\partial_\mu\Sigma^\dagger_{mn}\Sigma_{nj}-\Sigma^\dagger_{mn}\partial_\mu\Sigma_{nj})S_{R,k}]\\ &+\frac{k}{8f^3}\epsilon_{ijk}[\Sigma^{T\dagger}_{il}\bar{S}^{T\mu}_{lm}(\partial_\mu\Sigma_{mn}\Sigma^\dagger_{nj}-\Sigma_{mn}\partial_\mu\Sigma^\dagger_{nj})S_{L,k}]\\ &+\frac{\kappa f}{2M_{\Lambda_Q}}\epsilon_{ijk}\epsilon_{\mu\nu\rho\sigma}(\bar{S}^\mu_{il}\Sigma^\dagger_{lj}v^\nu\sigma^{\rho\sigma}S_{L,k}-\bar{S}^{T\mu}_{il}\Sigma_{lj}v^\nu\sigma^{\rho\sigma}S_{R,k})\\ &+\frac{r}{F^2}\epsilon_{ijk}(\bar{S}^\mu_{il}Q_{lm}\Sigma^\dagger_{mj}S_{L,k}+\bar{S}^{T\mu}_{il}Q_{lm}\Sigma_{mj}S_{R,k})v^\nu F_{\mu\nu}\\ &+\text{H.c.},\end{aligned} \tag{A4}$$

where $F_{\mu\nu}$ is the field strength of the photon and $\sigma_{\mu\nu}$ is defined as $\sigma_{\mu\nu}=\frac{i}{2}[\gamma_\mu,\gamma_\nu]$. The ρ meson dominance and the coupling universality suggest $k=1$ [5–7]. Here, M_{Λ_Q} denotes the masses of the ground state $\Lambda_Q(1/2^+)$, and F is a constant with dimension one. In this analysis, we take $F=350$ MeV following Ref. [13].

APPENDIX B: DECAY WIDTH OF A DIQUARK

In this appendix, we consider the decay width of a diquark corresponding to $\Lambda_Q(1/2^-)\to\Lambda_Q(1/2^+)\eta$ decay.

Let us first work in the chiral limit. The Lagrangian of the diquark is written as [1]

$$\begin{aligned}\mathcal{L}_{qq} =& \mathcal{D}_\mu d_{R,i}(\mathcal{D}^\mu d_{R,i})^\dagger+\mathcal{D}_\mu d_{L,i}(\mathcal{D}^\mu d_{L,i})^\dagger\\ &-m_0^2(d_{R,i}d^\dagger_{R,i}+d_{L,i}d^\dagger_{L,i})\\ &-\frac{m_1^2}{f}(d_{R,i}\Sigma^\dagger_{ij}d^\dagger_{L,j}+d_{L,i}\Sigma_{ij}d^\dagger_{R,j})\\ &-\frac{m_2^2}{2f^2}\epsilon_{ijk}\epsilon_{lmn}(d_{R,k}\Sigma_{li}\Sigma_{mj}d^\dagger_{L,n}+d_{L,k}\Sigma^\dagger_{li}\Sigma^\dagger_{mj}d^\dagger_{R,n}).\end{aligned} \tag{B1}$$

From the Lagrangian, we obtain the width of $qq(0^-)\to qq(0^+)\eta$ decay as

$$\Gamma_{qq}=\frac{1}{6\pi}\left(\frac{m_1^2+m_2^2}{f}\right)^2\frac{|\boldsymbol{p}|}{M(0^-)^2}, \tag{B2}$$

where $\boldsymbol{p}$ is the momentum of η, and $M(0^-)$ is the mass of the diquark with spin-parity 0^-. The GT relation of the diquark in the chiral limit is

$$\frac{m_1^2+m_2^2}{f}=\frac{[M(0^-)]^2-[M(0^+)]^2}{2f}, \tag{B3}$$

where $M(0^+)$ is the mass of the diquark with spin-parity 0^+. Using this relation, Eq. (B2) is rewritten as

$$\Gamma_{qq}=\frac{2}{3\pi}\left(\frac{M(0^-)-M(0^+)}{2f}\right)^2\left(\frac{M(0^-)+M(0^+)}{2M(0^-)}\right)^2|\boldsymbol{p}|. \tag{B4}$$

When $\langle\Sigma_{ij}\rangle=f\delta_{ij}$ is small compared with $M(0^+)$, we can take $|\boldsymbol{p}|\to M(0^-)-M(0^+)\equiv\Delta M_{qq}$ and $M(0^-)+M(0^+)\to 2M(0^-)$. Then, the decay width is expressed by the mass difference ΔM_{qq} as

$$\Gamma_{qq}=\frac{[\Delta M_{qq}]^3}{6\pi f^2}. \tag{B5}$$

On the other hand, the width of $\Lambda_Q(1/2^-)\to\Lambda_Q(1/2^+)\eta$ decay is obtained from the Lagrangian of SHBs (1) as

$$\Gamma_{qqQ}=\frac{2}{3\pi}\left(\frac{\Delta M}{2f}\right)^2\frac{M(1/2^+)}{M(1/2^-)}|\boldsymbol{p}|, \tag{B6}$$

where we used the GT relation in the chiral limit (16). In the heavy-quark limit, we can replace $|\boldsymbol{p}|\to\Delta M$ and $M(1/2^+)/M(1/2^-)\to 1$, and obtain

$$\Gamma_{qqQ}=\frac{[\Delta M]^3}{6\pi f^2}. \tag{B7}$$

Now, we can easily see a coincidence between Eqs. (B5) and (B7) with an approximation $\Delta M_{qq}\simeq\Delta M$.

Next, let us include the flavor symmetry breaking by $A>1$. The coupling constant of $ud(0^-)\to ud(0^+)\eta$ decay is obtained as

$$\begin{aligned}g_{ud}&=\frac{m_1^2+m_2^2}{f}=\frac{\Delta[M_{1,2}]^2+\Delta[M_3]^2}{2f(A+1)}\\ &=\frac{\Delta[M_3]^2}{2f}\frac{\frac{\Delta[M_{1,2}]^2}{\Delta[M_3]^2}+1}{A+1},\end{aligned} \tag{B8}$$

where $\Delta[M_i]^2=[M_i(0^-)]^2-[M_i(0^+)]^2$ $(i=1,2,3)$. From the inverse mass ordering $\Delta[M_{1,2}]^2<\Delta[M_3]^2$ and $A>1$, this coupling constant is smaller than the one expected from the GT relation of the diquark:

$$\bar{g}_{ud}=\frac{m_2^2}{f}=\frac{\Delta[M_3]^2}{2f}. \tag{B9}$$

Therefore, we expect that the effect of the anomaly suppresses the decay width of $ud(0^-)\to ud(0^+)\eta$, similarly to that of $\Lambda_Q(1/2^-)\to\Lambda_Q(1/2^+)\eta$.

Adopting the prescription of η-η' mixing in Sec. III, the coupling constant of $ud(0^-)\to ud(0^+)\eta$, including the effect of mixing, is obtained as

$$g^{\rm phys}_{ud}=\frac{\xi_1 m_1^2+\xi_2 m_2^2}{f}. \tag{B10}$$

For the inverse mass ordering, $|m_1^2|>|m_2^2|$, $m_1^2>0$, and $m_2^2<0$ hold [1]. Because $\xi_1<1$ and $\xi_2>1$ as shown in Sec. III, the effect of η-η' mixing also suppresses the decay

width compared with the one calculated from the coupling constant naively expected from the GT relation as

$$\bar{g}_{ud}^{\mathrm{phys}} = \frac{\xi_2 m_2^2}{f} = \xi_2 \bar{g}_{ud}. \tag{B11}$$

We numerically evaluate the decay width of $ud(0^-) \to ud(0^+)\eta$ by taking $M_{1,2}(0^+) = 906$ MeV and $M_3(0^+) = 725$ MeV [1,14]. We show the dependence of the $ud(0^-) \to ud(0^+)\eta$ width on $M_3(0^-)$ in Fig. 6. The vertical thick dashed red line is at $M_3(0^-) = 1329$ MeV estimated from $M(\Lambda_c(1/2^-)) = 2890$ MeV, while the vertical thick dash-dotted magenta line is at the threshold of the $ud(0^-) \to ud(0^+)\eta$ decay. The thin solid green and thin dotted orange curves are plotted without η-η' mixing. The thin solid green curve is drawn by using the coupling constant in Eq. (B8), which includes the effect of the anomaly, while the thin dotted orange curve is drawn by using the one in Eq. (B9) without anomaly. The thick solid blue and thick dotted purple curves include the effect of η-η' mixing. The thick solid blue curve is drawn by using the coupling constant in Eq. (B10), which includes the effect of the anomaly, while the thick dotted purple curve is drawn by using the one in Eq. (B11). From Fig. 6, we see the suppression from the effects of anomaly and η-η' mixing, similarly to the SHBs shown in Figs. 1 and 2. Because $[(M(0^-) + M(0^+))/2M(0^-)]^2$ in Eq. (B4) is smaller than $M(1/2^+)/M(1/2^-)$ in Eq. (B6), the widths of the diquark shown by the thin dotted orange and thick dotted purple curves are smaller than those of the SHBs in Figs. 1 and 2.

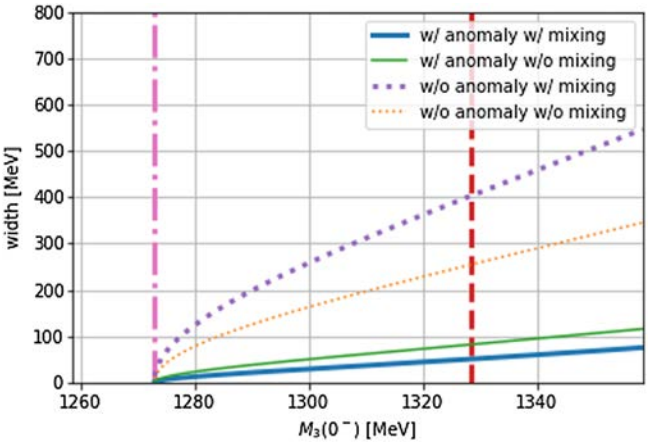

FIG. 6. Dependence of the $ud(1/2^-) \to ud(1/2^+)\eta$ decay width on $M_3(0^-)$. The curves correspond to those in Fig. 1.

[1] M. Harada, Y. R. Liu, M. Oka, and K. Suzuki, Phys. Rev. D **101**, 054038 (2020).
[2] T. Yoshida, E. Hiyama, A. Hosaka, M. Oka, and K. Sadato, Phys. Rev. D **92**, 114029 (2015).
[3] M. Tanabashi *et al.* (Particle Data Group), Phys. Rev. D **98**, 030001 (2018).
[4] Y. Kim, E. Hiyama, M. Oka, and K. Suzuki, Phys. Rev. D **102**, 014004 (2020).
[5] J. J. Sakurai, *Currents and Mesons* (University of Chicago Press, Chicago, USA, 1969).
[6] M. Bando, T. Kugo, and K. Yamawaki, Phys. Rep. **164**, 217 (1988).
[7] M. Harada and K. Yamawaki, Phys. Rep. **381**, 1 (2003).
[8] M. Harada, M. Rho, and C. Sasaki, Phys. Rev. D **70**, 074002 (2004).
[9] M. Harada and J. Schechter, Phys. Rev. D **54**, 3394 (1996).
[10] Y. Kawakami and M. Harada, Phys. Rev. D **97**, 114024 (2018).
[11] Y. Kawakami and M. Harada, Phys. Rev. D **99**, 094016 (2019).
[12] V. Dmitrašinović and H. X. Chen, Phys. Rev. D **101**, 114016 (2020).
[13] P. L. Cho, Phys. Rev. D **50**, 3295 (1994).
[14] Y. Bi, H. Cai, Y. Chen, M. Gong, Z. Liu, H. X. Qiao, and Y. B. Yang, Chin. Phys. C **40**, 073106 (2016).